Cytometry Part A

ISAC CYTOMETRY Journal of Quantitative Cell Science PART A

ORIGINAL ARTICLE OPEN ACCESS

EGFR-HER2 Transactivation Viewed in Space and Time Through the Versatile Spectacles of Imaging Cytometry—Implications for Targeted Therapy

László Ujlaky-Nagy[1,2] | János Szöllősi[1,2] | György Vereb[1,2,3]

[1]Department of Biophysics and Cell Biology, Faculty of Medicine, University of Debrecen, Debrecen, Hungary | [2]HUN-REN–DE Cell Biology and Signaling Research Group (Hungarian Research Network - University of Debrecen), Faculty of Medicine, University of Debrecen, Debrecen, Hungary | [3]Faculty of Pharmacy, University of Debrecen, Debrecen, Hungary

Correspondence: György Vereb (gvereb2020@gmail.com)

Received: 27 September 2024 | **Revised:** 3 December 2024 | **Accepted:** 24 January 2025

Funding: This work was supported by the National Research, Development, and Innovation Office, Hungary (OTKA K143771, GINOP-2.3.3-15-2016-00003); Hungarian Research Network; University of Debrecen Program for Scientific Publication.

Keywords: Airyscan microscopy | confocal microscopy | epidermal growth factor receptor | ErbB2 | fluorescence correlation spectroscopy | fluorescence cross-correlation spectroscopy | Fluorescence lifetime imaging microscopy | Förster resonance energy transfer | HER2

ABSTRACT

Ligand-induced formation of signaling platforms composed of homo- and/or heterodimers of receptor tyrosine kinases is considered essential for their activation and consequential contribution to the progression of many cancers. Epidermal Growth Factor Receptor (EGFR) acts as a signal receiver upon EGF binding and produces mitogenic input for many cells also through receptor-heterodimerization with its ligandless partner, Human Epidermal growth factor Receptor 2 (HER2). Ligand-driven transactivation is a key step leading to changes in the cell surface pattern of EGFR and HER2; their interaction plays a key role in various malignancies, especially when HER2 molecules are overexpressed. Our clinically relevant model system is the SK-BR-3 breast tumor cell line, overexpressing HER2 and moderately expressing EGFR. This cell line shows significant dependency on EGF-driven HER2 signaling. We studied changes in the interaction between EGFR and HER2 in the cell membrane upon EGF binding, applying various biophysical approaches with different time scales. Changes in molecular proximity were characterized by fluorescence lifetime imaging microscopy (FLIM) techniques assessing Förster resonance energy transfer (FRET), which confirmed the ligand-enhanced interaction of EGFR and HER2, followed by an increase in HER2 homoassociation. EGF binding and transactivation were reflected in the phosphorylation of both receptor types as well. At the same time, superresolution Airyscan microscopy and fluorescence correlation and cross-correlation spectroscopy (FCS/FCCS), sensitive to changes in the size of stationary and diffusing aggregates, respectively, have revealed cyclic increases in the aggregation and stable co-diffusion of membrane-localized HER2, possibly caused by internalization and recycling, eventually leading to a new equilibrium. Such dynamic fluctuation of receptor interaction may open a window for the binding of therapeutic antibodies that are aimed at inhibiting heterodimerization, such as pertuzumab. The complementary array of state-of-the-art imaging cytometry approaches thus demonstrates a spatiotemporal pattern of spontaneous and induced receptor aggregation states that could provide mechanistic insights into the potential success of targeted therapies directed at the HER family of receptor tyrosine kinases.

Abbreviations: EGF, Epidermal growth factor; EGFR, Epidermal growth factor receptor; FCCS, Fluorescence cross-correlation spectroscopy; FCS, Fluorescence correlation spectroscopy; fd-FLIM, Frequency-domain FLIM; FLIM, Fluorescence lifetime imaging microscopy; FRET, Förster resonance energy transfer; HER2, Human epidermal growth factor receptor 2; PCH, Photon count histogram; TCSPC, Time correlated single photon counting; td-FLIM, Time-domain FLIM.

1 | Introduction

One of the best-studied families of transmembrane receptor tyrosine kinases (RTKs) is the family of human epidermal growth factor receptors (HER, or ErbB (Erythroblastosis B) family). It includes the epidermal growth factor receptor EGFR (HER1), HER2, which has no known physiological ligand, HER3, whose kinase activity is impaired, and HER4. The differentiation, survival, and proliferation signals from these members are essential for normal and cancer cells [1–5]. Their mechanism of action involves homo- and heteroassociation, forming active dimers through dimerization domains. Dimerization of the extracellular domains is followed by conformational coupling across the membrane, promoting the formation of catalytically active asymmetric kinase dimers that trans-phosphorylate the C-terminal tails, which serve as docking sites for proteins containing SH2/PTB domains and initiate downstream signaling [6, 7].

The expression levels of HER family members, their homo- and heteroassociations, spatiotemporal interaction, phosphorylation pattern, and localizations on the cell surface or inside the cells yield diverse biological functions [8, 9]. The ligandless HER2 is a frequent heterodimerization partner for the EGFR, and their interaction is implicated in various human cancers [10]. The importance of HER2 is highlighted by the fact that whenever HER2 is involved in the heterodimer formation, the mitogenic potential is increased. Gene amplifications leading to overexpression as well as mutations of the kinase domain resulting in increased activity have been described for both EGFR and HER2 [11–14]. Importantly, the dimerization arm in the EGFR ectodomain is autoinhibited by its own structure without ligand binding. This regulation by ligand-dependent conformational changes seems to be ubiquitous in the HER family, excepting the case of HER2, which renders HER2 constitutively active [15–19].

In parallel with in vitro observations, early literature data on HER2 expression patterns and their connection to clinical consequences about therapy resistance also support the prominent role of HER2 [20]. While EGFR is most often connected to non-small cell lung cancer and colorectal cancer [21], HER2 is frequent in gastric, bladder, and breast cancers [22]. When the two are co-expressed, EGFR may serve as an essential signal-antenna for the ligandless HER2 in their heterodimers: their over- and co-expression in bladder cancer was reported for the majority of the tumors and metastases [23]. Furthermore, 20% of breast cancer cases are characterized by a moderate expression level of EGFR together with the overexpression of HER2. In addition to intratumor heterogeneity of expression [24, 25], the interaction of these two kinases may be related to progression [26] and metastatic ability [27] of these tumors even when humanized antibodies such as trastuzumab [28], its maytansinoid conjugate, TDM-1 [29], or pertuzumab [30] are employed as specific HER2-targeting therapy.

Intermolecular interactions of EGFR and HER2 have been investigated by applying Förster Resonance Energy Transfer (FRET). FRET-related methods and techniques are based on a photophysical phenomenon taking place between donor and acceptor fluorescent dyes [31]. As FRET efficiency shows high distance dependence in the range of 1–10 nm, measuring FRET reveals molecular distances far beyond the resolution afforded by diffraction-limited conventional optical microscopy [32]. The approaches exploiting FRET include monitoring changes in intensities of donor and acceptor emission signals, excited state lifetime, or just considering donor intensity changes, donor or acceptor depletion kinetics, or anisotropy [33–40]. Of these, time-domain and frequency-domain fluorescence lifetime imaging (FLIM-FRET) techniques are the most direct ways to measure FRET, having several advantages compared to methods based on intensities or intensity ratios [41]. They are relatively insensitive to local fluorophore concentrations, sufficiently sensitive even at low concentrations of fluorescence species when used with appropriate donor-acceptor pairs, need to be measured only for the donor dye, and require minimal corrections [42]. However, all techniques also have their restrictions. In the majority of time-domain measurements, which employ raster scanning of a single focal point, relatively long acquisition times limit application to the examination of fixed samples [43, 44]. On the other hand, since most frequency-domain lifetime microscopes operate in widefield mode, the simplest measurement with these done at a single modulation frequency optimized for the excited state lifetime of the fluorophore is fast enough to allow the investigation of living cells [45]. However, if the fluorophore has more than one lifetime component, or there is spectral spillover from the acceptor dye or considerable auto-fluorescence, then a multi-frequency approach is needed to increase accuracy, which reduces the time resolution of monitoring events in living cells.

Another useful method for analyzing molecular interactions in situ in cells is fluorescence correlation spectroscopy (FCS) which can assess fluorescence fluctuations originating from the movement of small molecular ensembles in a subfemtoliter volume and combines sensitivity and low background with high statistical confidence [46], even in biological systems and cells [47–51]. In FCS, an autocorrelation function is generated, which can distinguish smaller and larger molecular aggregates if their diffusion constants are sufficiently different to be represented by distinguishable diffusion correlation times in the function. This in practice means a factor of at least two, generally requiring differences in molecular weights by a factor of four to eight. While this allows sensitive detection of smaller species binding to molecules that are at least an order of magnitude larger [52], the potentially continuous spectrum of the level of receptor aggregation and/or lower degrees of oligomerization (e.g., dimerization) is not well resolved. Viable strategies for such cases are the calculation of the average molecular brightness of the diffusing species [51] or the generation of photon count histograms from the fluctuation traces [53] when using a single optical channel. By introducing two spectrally well-separated channels, fluorescence cross-correlation spectroscopy (FCCS) also obviates these limitations while still affording the assessment of diffusion constants [54, 55]. With its inherent sensitivity for synchronous events, it allows detection of co-diffusion of receptors labeled with different fluorescence species that could reflect obvious interactions, which are stable at least during the time that the particles dwell in the observation volume [56, 57].

In the present work, we have explored EGFR and HER2 interactions and clustering on the cell surface in relationship to EGF stimulation. Our model system was the SK-BR-3 breast tumor cell line, which overexpresses HER2 [58] and moderately expresses EGFR [59]. It is moderately sensitive to the

HER2-targeted therapeutic antibody trastuzumab (Herceptin) [60]. We found using FLIM-FRET that EGF induced an increase in the heteroassociation of EGFR and HER2 and homoassociation of HER2 within minutes, which was followed by increased phosphorylation of EGFR and HER2 on the same time scale. EGF stimulation also increased the size of HER2 clusters, as revealed by Airyscan superresolution microscopy and FCS. FCCS showed that EGF also enhanced stable HER2 co-diffusion. The stimulus-induced molecular aggregation showed a cyclic change until a new equilibrium was reached, indicating the role of receptor internalization and recycling and hinting that this spatiotemporal dynamics could influence the binding ability of therapeutic antibodies and the effect of other targeted therapies that interfere with dimerization-based receptor activation.

2 | Materials and Methods

All materials were from Sigma-Aldrich (MilliporeSigma, Burlington, MA, USA) unless otherwise indicated. Thermo Fisher denotes Thermo Fisher Scientific, Waltham, MA, USA throughout.

2.1 | Cell Culture

The SK-BR-3 cell line was obtained from the American Type Culture Collection (ATCC, Rockville, MD, USA) and cultured according to specifications in a humidified atmosphere with 5% CO_2 at 37°C in Dulbecco's Minimal Essential Medium supplemented with 10% fetal calf serum and antibiotics. Expression of EGFR (100,000 molecules per cell) and HER2 (800,000 molecules per cell) was confirmed using a Qifikit (Dako, Glostrup, Denmark) standard. Cells were propagated every 2 to 3 days, seeded 36–48 h before use into ibidi μ-Slide 8 well chambers (ibidi GmbH, Gräfelfing, Germany) for live cell measurements, onto coverslips for time-domain lifetime imaging, or into cell culture grade Petri dishes (Eppendorf AG, Wien, Austria) for Western blotting, and allowed to grow to 75%–80% confluence. Prior to measurements, cells were kept in serum-free HEPES buffer (20 mM HEPES, 123 mM NaCl, 5 mM KCl, 1.5 mM MgCl2, 1 mM CaCl2, 10 mM glucose, pH 7.2) supplemented with 10 mM glucose for 2 h. Human recombinant EGF was used for stimulation at a final concentration of 100 nM.

2.2 | Immunofluorescent Labeling

EGFR was labeled with the ab-11 mouse monoclonal antibody (ThermoFisher); HER2 was labeled with the Fab fragment of Mab76.5. The hybridoma line producing 76.5 was a kind gift from Yosef Yarden, Weizmann Inst. of Science, Rehovot, Israel. Antibody purification and Fab fragment preparation were performed according to standard protocols. Antibodies and Fab fragments were conjugated with Alexa Fluor 488 (AF488), Alexa Fluor 546 (AF546), Alexa Fluor 647 (AF 647), or Cy3 NHS succinimidyl ester (Invitrogen, ThermoFisher) according to the manufacturer's protocol. Cells were then labeled for the times indicated for each measurement type using a saturating antibody concentration of 5 μg/mL determined from dose titration. For samples that were fixed after labeling, all washing and labeling steps were carried out on an ice-cold surface and in HEPES buffer. For live cell measurements, labeling was done at 37°C, and the HEPES buffer used was supplemented with 10 mM glucose. Labeling of cells was terminated with a wash in excess HEPES buffer.

2.3 | Time-Domain FLIM-FRET Measurement

Cells on coverslips were stimulated with EGF for 2, 3, 5, 10, or 15 min at 37°C. A wash with ice-cold HEPES buffer was used to stop further reaction. EGFR and HER2 were then labeled on ice for 15 min with AF546-conjugated ab-11 as FRET donor and AF647-conjugated 76.5 Fab as FRET acceptor. Labeled cells were fixed with ice-cold formaldehyde (2%) for 10 min and allowed to warm to room temperature for another 10 min before rinsing and mounting in Mowiol antifade comprising 0.1 M TrisHCl, pH 8.5, 25% (w/v) glycerol, and 10% Mowiol 4–88 (Polysciences, Warrington, PA, USA).

Donor fluorescence-lifetime imaging (FLIM) was done in the time-domain by time-correlated single photon counting (TCSPC) on confocal membrane slices of the fixed cells using a Nikon Eclipse T12 confocal microscope with a C-Apochromat 63x/1.2 NA water immersion objective (Nikon Solutions Co. Ltd., Tokio, Japan). Donor and acceptor images were taken intermittently and analyzed with PicoQuant SymPhoTime-64 (PicoQuant, Berlin, Germany). Acquisition parameters were as follows: excitation: 560 nm, 8 μW, 20 MHz repetition rate; emission: 595/50 nm bandpass filter, TCSPC integration time was 5 min for Nyquist-sampled 512 × 512 pixel images, with a cumulative pixel dwell time of 1.144 ms. A single component τ lifetime model with iterative fit provided accurate fitting, further one or two components did not improve the χ^2 parameter. For all fit models, the τ_{AvAmp} amplitude-weighted average lifetime was calculated after Instrument Response Function calibration:

$$\tau_{\mathrm{AvAmp}} = \frac{\sum_{k=0}^{n-1} A[k]\tau[k]}{A_{\mathrm{sum}}}. \quad (1)$$

The average E FRET efficiency was calculated for each cell labeled with both donor and acceptor using all pixels of the cell's membrane that showed τ_{AvAmp} lifetimes in the range of 0.5–10 ns as:

$$E = \left[1 - \frac{\tau_{\mathrm{AvAmp}}}{\tau_D}\right]. \quad (2)$$

where τ_D was average τ_{AvAmp} for the samples labeled with donor only and [] represents averaging.

2.4 | Frequency-Domain FLIM-FRET Measurement

For following in real time HER2 homodimerization in live cells, SK-BR-3 cells were labeled with AF488-conjugated 76.5

Fab fragments (donor only reference sample) or also with Cy3-conjugated 76.5 Fab antibody fragments (donor + acceptor FRET sample) for 5 min. A Lambert Instruments (Groningen, The Netherlands) LIFA device using the modulated Multi-LED light source, mounted on an Olympus IX81 microscope with an Olympus PlanSApo 60x; NA: 1.2 W objective, was used for wide-field imaging. For 25 mins, two lifetime images per minute were acquired, each based on 12 phase images in random sequence, at a 40 MHz modulation frequency, and a resolution of 640 × 528 pixels with 2 × 2 binning. For excitation, the 470–490 nm LED was used, and emission was detected through a 530/40 nm band-pass filter. Cells were stimulated with EGF after taking a 5-min baseline. To determine FRET efficiency, it was considered that for the donor only sample, intensity after a pulse excitation decays as:

$$I(t) = \alpha e^{-t/\tau_D}, \tag{3}$$

Whereas if in the same pixel acceptor molecules are present and FRET occurs, the emission decay is modified asfollows:

$$I(t) = \alpha_D e^{-t/\tau_D} + \alpha_{\mathrm{DA}} e^{-t/\tau_{\mathrm{DA}}}; \tag{4}$$

where $\alpha_D, \alpha_{\mathrm{DA}}$ are amplitudes representing donor with and without FRET acceptors, respectively, and $\tau_D, \tau_{\mathrm{DA}}$ are the actual lifetimes of the donor in the absence and presence of FRET. The average FRET efficiency for any set of pixels is calculated as:

$$E = 1 - \frac{\langle \tau_{\mathrm{obsDA}} \rangle}{\langle \tau_{\mathrm{obs}D} \rangle} \tag{5}$$

where $\langle \tau_{\mathrm{obsD}} \rangle$ is the observed lifetime averaged from several donor-only samples, and $\langle \tau_{\mathrm{obsDA}} \rangle$ is the average observed lifetime in the region of interest of the sample labeled both with donor and acceptor. ROIs were gated for above-background donor intensity and the 95% confidence interval of the lifetime histograms. Analysis was done with the LI-FLIM 1.1.24 program (Lambert Instruments) and observed lifetimes presented are based on the phase shift of emission.

2.5 | Fit-Free Phasor Representation of Frequency-Domain Fluorescence Lifetime Measurement (fd-FLIM)

The phasor approach to fd-FLIM-FRET could markedly reduce analysis complexity and could provide a powerful visualization of the data content [61]. Fit-free representation in a phasor plot contains information on many thousands of pixels. Data obtained from each pixel were converted to phasor plot points by the following transformation [61–64]:

$$g_{i,j}(\omega) = m_{i,j}\cos\left(\phi_{i,j}\right) \tag{6}$$

and

$$s_{i,j}(\omega) = m_{i,j}\sin\left(\phi_{i,j}\right) \tag{7}$$

Where $m_{i,j}$ and $\phi_{i,j}$ are the modulation and phase shift of the emission signal, respectively, at pixel i, j, ω is the angular frequency of excitation and the g and s coordinates are the projections of the polar coordinates in the coordinate axes. In the case of a single exponential decay, transformed phasor co-ordinates can also be expressed as follows:

$$g_{i,j}(\omega) = \frac{1}{1 + \left(\omega\tau_{\mathrm{obs}}\right)^2}, \tag{8}$$

and

$$s_{i,j}(\omega) = \frac{\omega\tau_{\mathrm{obs}}}{1 + \left(\omega\tau_{\mathrm{obs}}\right)^2}, \tag{9}$$

where τ_{obs} is the observed donor lifetime, and consequently

$$s^2{}_{i,j} + \left(g^2{}_{i,j} - \frac{1}{2}\right)^2 = \frac{1}{4}, \tag{10}$$

which implies that all single exponential lifetimes will fall on a semicircle of radius 1/2 and center (1/2; 0): shorter lifetimes are localized closer to the point (1, 0) (which corresponds to $\tau = 0$); whereas longer lifetimes are closer to (0, 0) (corresponding to $\tau = \infty$). As phasors follow the rule of linear addition, in a heterogeneous sample where a single pixel comprises a mixture of non-FRET-ting and FRET-ting fluorescence species, it has a position inside the universal circle: the higher the FRET efficiency, the more inside and closer to the right corner the point will be. Phasor plots were prepared in the LI-FLIM 1.1.24 program.

2.6 | Measuring HER2 Oligomerization With Airyscan Superresolution Microscopy

Cells were labeled with AF647-conjugated 76.5 Fab fragments (5 μg/mL, 37°C, 5 min). Airyscan images from 600 nm optical slices of the apical membrane surface were acquired immediately (starting point) and 5, 10, 15, and 35 min after EGF ligand stimulus using an LSM 880 confocal laser scanning microscope (Carl Zeiss AG, Oberkochen, Germany) equipped with a water immersion objective (C-Apochromat 40×, NA 1.2) and an Airyscan detection unit. Excitation was with a 633 nm He-Ne laser, and emission was detected through a 488/543/633 triple beam splitter and a 640 nm longpass filter. ZEN Blue 2.1 software was used to process each of the 32 Airy detector channels separately by performing filtering, deconvolution, and pixel reassignment. Wiener filter deconvolution with a 2D reconstruction algorithm was applied. The size distribution of receptor clusters was determined in ImageJ/Fiji by applying a common stack threshold to each time series and using the built-in analyze particles function. Pixel size distributions were plotted on a logarithmic scale and were compared with the χ^2 test.

2.7 | Fluorescence Correlation and Cross-Correlation Spectroscopy (FCS and FCCS)

To determine the diffusion characteristics of membrane HER2 molecules, live cells were labeled with 1 μg/mL of AF488 and/

or AF647 conjugated 76.5 Fab fragments for 5 min at 37°C and washed twice. The concentration of Fab fragments was titrated for optimal brightness while avoiding internalization during the observation time range. Using the Zeiss LSM 880 (described under 2.6), a fast confocal Z-stack was acquired first to locate the apical membrane sections distal from the bottom of the chamber and to set the subfemtoliter excitation volume overlapping with the membrane. A 5 s pre-bleaching of the immobile fraction of fluorophores was followed by FCS/FCCS data collection. Excitation was with the 488 nm (13 μW) and 633 nm (19 μW) laser lines, detection through a 488/543/633 triple beam splitter on the 32-element GaAsP array in the 495–548 and 642–695 nm ranges in photon counting mode.

FCS data collection time period of one confocal volume on one cell was 10 s repeated 10 times [65] before moving to another cell in the same well. This allowed acquiring the necessary data from any given cell in every 2–3 min. Owing to this time constraint, cellular data from independent experiments were pooled into the best matching 5-min-long time slots. EGF stimulation was done after obtaining a few control traces in ~15 min.

The fluctuation of fluorescence intensity produced by the diffusion of labeled membrane-HER2 in the sub-femtoliter volume was measured, and an autocorrelation function was generated:

$$G_{I(\tau)} = \frac{\langle I_{(t)} I_{(t+\tau)} \rangle}{\langle I_{(t)} \rangle^2}, \tag{11}$$

where t indicates any time point during acquisition, and τ the various time delays for which correlation was computed. The operator $\langle\ \rangle$ indicates averaging over the whole range of data. In the case of cross-correlation analysis (FCCS), HER2 molecules in the membrane were labeled with a 1:1 mixture of 76.5 Fab fragments conjugated exclusively with either AF488 or AF647. Verifying strong co-localization of the labels on confocal images was followed by the collection of intensity fluctuation time traces in both channels. From these fluctuations, autocorrelation and cross-correlation functions were generated:

$$G_{Ix(\tau)} = \frac{\langle I_{gr(t)} I_{r(t+\tau)} \rangle}{\langle I_{gr(t)} \rangle \langle I_{r(t)} \rangle} \tag{12}$$

Here, the variables matching those in the autocorrelation function, except the I intensity in one spectral channel (gr for green emission in our case) is correlated with the signal in the other channel (r for red emission in our case) at various τ delays. For a thorough analysis, the cross-correlation in the other direction, using $\langle I_{r(t)} I_{gr(t+\tau)} \rangle$ in the numerator was also calculated.

For fitting the autocorrelation and cross-correlation functions, the 10 curves from the same spot were averaged. Three diffusing components were fitted; the quick 3D diffusion of unbound fluorescently conjugated Fab fragments was fitted with a free 3D model (1), while the fast membrane diffusion of labeled monomers/dimers (2) slow membrane diffusion of higher aggregates (3) were both fitted with an anomalous 2D model. Triplet transition was also accounted for, yielding the overall model of

$$G_{\mathrm{tot}(\tau)} = 1 + G_{\mathrm{triplet}(\tau)} G_{D(3\mathrm{comp})(\tau)}, \tag{13}$$

where

$$G_{\mathrm{triplet}(\tau)} = \frac{\left(1 - T + Te^{-\tau/\tau_{tr}}\right)}{1 - T}. \tag{14}$$

and

$$\begin{aligned} G_{D(3\mathrm{comp})(\tau)} &= G_{\mathrm{free}3D(\tau)} + G_{\mathrm{anomal}2D(\tau)} \\ &= \frac{\phi_1}{\left(1 + \frac{\tau}{\tau_{d1}}\right)\left(1 + \frac{\tau}{\tau_{d1}} \frac{1}{S^2}\right)} + \sum_{i=2}^{3} \frac{\phi_i}{\left(1 + \left(\frac{\tau}{\tau_{di}}\right)^{\alpha_i}\right)}. \end{aligned} \tag{15}$$

where ϕ_i is the fractional intensity of the i^{th} component; $\tau_{d,i}$ is the diffusional correlation time of the i^{th} component, that is, the characteristic time the particle spends in the confocal volume—the longer it is, the slower the diffusion is; S is a structural parameter relating the z axis of the observation volume to the x/y axes (~ 7 in our case); and α_i is an anomaly parameter for describing anomalous (hindered or facilitated) diffusion, which in our case was unity, indicating free diffusion. The average number of diffusing/co-diffusing species in the observation volume was calculated as $1/G_{\mathrm{anomal\ 2D}(\tau)}$. To characterize the tendency of stable association manifested in co-diffusion, the average number of co-diffusing species was normalized to the number of total diffusing species, using both spectral channels and comparing the two results. For evaluating cross-correlation, the triplet and free antibody components were omitted, as these are not expected to cross-correlate. Analysis was done with Zen Black 2.1 software (Carl Zeiss AG, Oberkochen, Germany).

2.8 | Generation of the Photon Count Histogram (PCH)

The average photon count $\langle k \rangle$, that is brightness of the fluorescence species (where a monomer or a large aggregate equally counts as a single species) was calculated as:

$$\langle k \rangle = \varepsilon \frac{V_{\mathrm{PSF}}}{V_0}, \tag{16}$$

where ε, the molecular brightness, is defined as

$$\varepsilon = I_0^N \beta \eta_w T. \tag{17}$$

Here V_{PSF} is the illumination volume; V_0 is the sample volume; T is the integration time increment; η_w is the detection efficiency; I_0 is the maximum excitation when the fluorophore is at the center of the illuminated volume; and β is a constant incorporating excitation probability, quantum yield, and instrument bias. Analysis was done with Zen Black 2.1 software.

2.9 | Western Blotting

Cells were stimulated with EGF for 0, 2, 5, or 10 min; then, after a quick wash, were harvested with a rubber policeman

into ice-cold lysis buffer comprising 20 mM Tris, 1% NP-40, 137 mM NaCl, 2 mM EDTA, 10% glycerol, pH 8.0, freshly added 2 mM Na-ortho-Vanadate, 1 mM PMSF, dithiothreitol, and protease inhibitor cocktail (cOmplete Mini Tablets, Roche, Basel, Switzerland). Lysates, mixed and boiled with sample buffer, were separated electrophoretically on SDS gel (8%, approximately 1.5 h, 120 V). A Bio-Rad (Bio-Rad Hungary Ltd., Budapest, Hungary) wet blotting system was used to transfer proteins onto PVDF-Immobilon P membranes (Millipore, Burlington, MA, USA). Membranes were blocked in TRIS buffer with 0.1% Tween 20 (TBS) supplemented with 5% non-fat milk powder for 1 h at room temperature. Primary antibodies anti-HER2 (cneuAB3/OP15), anti-pHER2 (cerbB2 Ab18—PN2A, ThermoFisher), anti-EGFR (MAP clone F4, ThermoFisher) and anti-pEGFR (1H12, Cellsignalling, Danvers, MA, USA) were used at 1 μg/mL in TBS with 1% milk powder overnight. The solvent was used to wash the membranes 3 times and to apply the peroxidase-conjugated anti-mouse secondary antibody (Jackson ImmunoResearch Europe, Ely, UK) at 1 μg/mL for 2 h at room temperature. Immunostaining was detected using enhanced chemiluminescence (ECL) reagent (Supersignal West Pico, ThermoFisher) and captured with a Multilmage III, Alpha (Innotech Corp., San Leandro, CA, USA). Quantitation was done in ImageJ/Fiji.

2.10 | Statistical Evaluation of Data

For comparison, either an unpaired t test or one-way ANOVA together with Dunnett's or Tukey's post hoc analysis was performed depending on the number of groups. Distributions were compared with the χ^2 test. For statistical analysis, Systat SigmaStat 3.5 was used. Plotting was done with MS Excel 2016, Graphpad Prism 5.03, Systat TableCurve 2D 5.01, or Systat SigmaPlot 10.0. Nonsignificant "p" values (> 0.05) are indicated by the abbreviation "N.S.," whereas "p" values < 0.05, < 0.01, and < 0.001 are denoted with asterisks, *, **, and ***, respectively.

3 | Results

3.1 | EGF Enhances Molecular Interaction Between EGFR and HER2

Since HER2 activation is enhanced by EGF-bound EGFR, the molecular interaction underlying this transactivation was investigated by time-domain fluorescence lifetime imaging-based Förster resonance energy transfer (td-FLIM-FRET) in confocal microscopy. SK-BR-3 cells were fixed and then labeled at 0, 2, 3, 5, 10, and 15 min after the addition of EGF. In the case of control cells (0 min stimulus), the FRET efficiency value was 7.9%, indicating that a significant portion of EGFR was in close molecular proximity to HER2 even in unstimulated cells. FRET efficiency was significantly increased by stimulating the cells with EGF: the efficiency went up to 17.3% at 3 min post-stimulation time ($p \leq 0.01$). This transiently enhanced interaction was gradually decreased from 5 min after stimulation, as indicated by the decrease in FRET efficiency, back to the initial baseline by 10 min, then tendentiously increased again, albeit this increase was not mathematically significant (Figure 1).

3.2 | HER2 Cluster Size Distribution Reveals Large-Scale Aggregation Enhanced by EGF

Next, we wanted to investigate how EGF stimulation influences the cluster formation of HER2 molecules. Toward this end, Airyscan confocal images were acquired on live SK-BR-3 cells from the top membrane slices labeled with fluorescent dye conjugated 76.5 Fab antibody fragments (Figure 2A). (In control experiments, Fab fragments were tested and showed no interference with dimerization, signaling, transactivation and aggregation.) In the presented experiments, the same membrane slices for each cell were monitored at several time points before and after the addition of EGF. The distribution of HER2 cluster size (measured by the number of pixels in each segmented cluster) is plotted on a logarithmic scale for the control and at 5 min after the EGF stimulus in Figure 2B. The increase in the size of HER2 clusters was significant at 5 min, as evidenced by a χ^2 test. As post-labeling time increased, the larger clusters slowly disappeared from the cell membrane, and after 15 min, the median cluster size returned to baseline. Notably, by 25 min, the larger clusters became more abundant again, followed by a new decline in median cluster size (Figure 2C). During the observed time interval, the cluster size distribution of HER2 on control (non-stimulated) cells did not change significantly.

3.3 | HER2-HER2 Molecular Interaction Increased by Ligand-Activated EGFR

HER2-HER2 molecular proximity was monitored by frequency-domain fluorescence lifetime imaging microscopy (fd-FLIM-FRET). We have chosen the fd-FLIM FRET because we wanted to follow the dynamics of homoassociation of HER2 in live cells. The average lifetime was 3.4 ns for donor-only samples, 3.2 ns for samples labeled with both donor and acceptor, and this decreased to 2.9 ns upon EGF stimulus within 5 min (Figure 3A). Phasor plots for the same samples are displayed in Figure 3B. The stepwise shift of the cluster of pixels to the right and inwards from the universal semicircle upon introducing the acceptor (middle frame) and further upon EGF stimulus (rightmost frame) indicates that in addition to maintaining donor-labeled receptors with no molecular proximity to acceptor-labeled receptors, an increasing number of donors undergo FRET and consequential shortening of their lifetime. Calculated FRET values are presented in Figure 3C. The first panel shows that the mean of FRET E from thresholded cellular averages increases to 14% from the baseline of 11% in 5 min after EGF stimulation and steadily increases up to 17% by 20 min.

3.4 | EGF Induced Dynamic Redistribution of HER2 Membrane Clusters Characterized by Fluorescence Correlation Spectroscopy (FCS)

The extracellular domain of HER2 was labeled with AF647 conjugated 76.5 Fab fragments to observe signal fluctuations (Figure 4A) originating from the diffusion of receptors in and out of the observation volume. The autocorrelation curves generated from thesefluctuations (Figure 4B, solid black trace) were

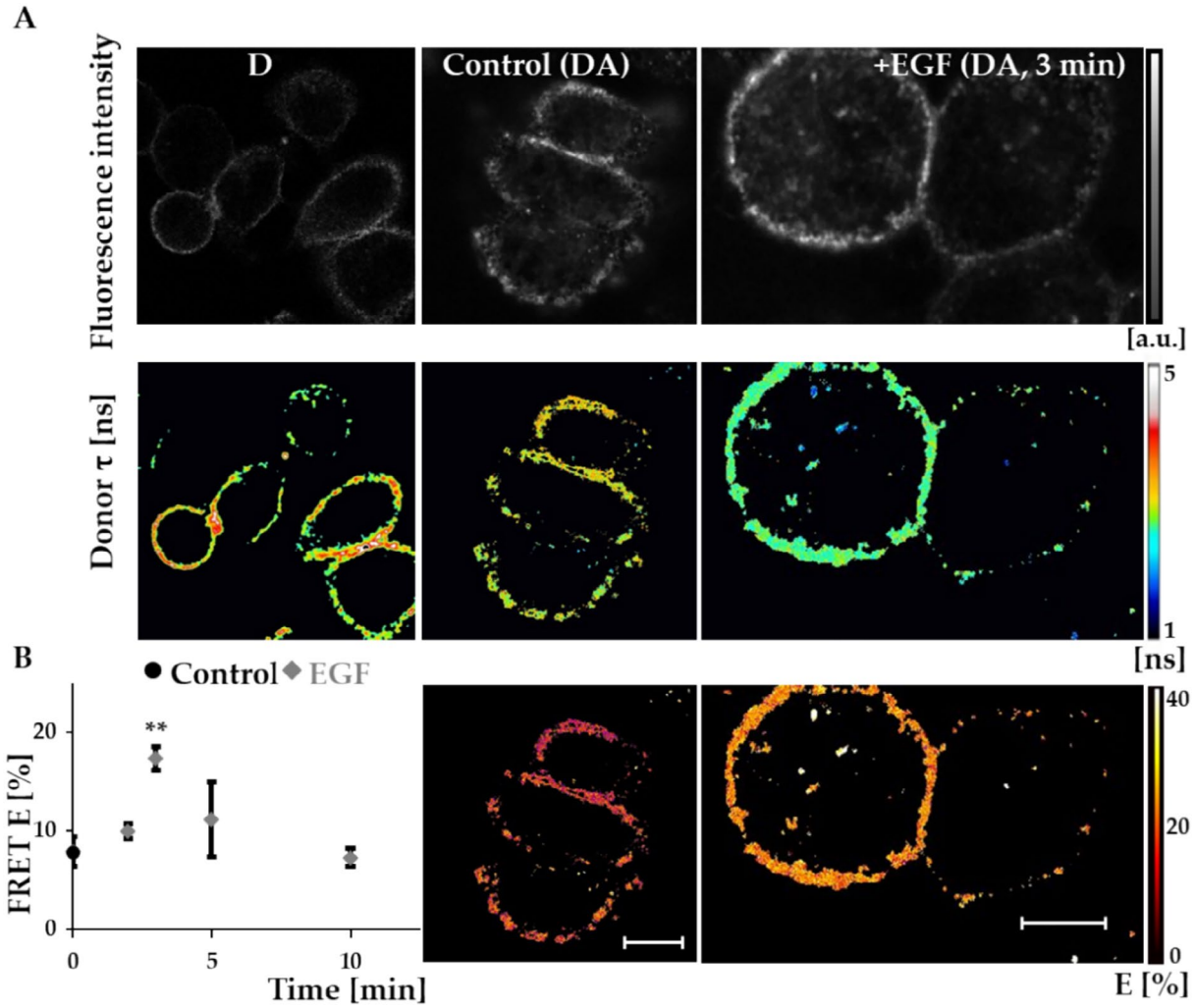

FIGURE 1 | EGFR-HER2 transient interaction induced by EGF. (A) Acquired donor intensity images of EGFR. EGFR was labeled with AF546 conjugated ab-11 (donor), HER2 with AF647 conjugated 76.5 Fab (acceptor). The panels show the donor only, donor + acceptor, and the donor + acceptor in the presence of EGF samples. (B) Donor lifetime images of labeled EGFR thresholded by donor intensities. (C) Cell-based average FRET efficiencies (mean ± SEM) were plotted before adding EGF (control) and at 2, 3, 5, 10, and 15 min after adding EGF (first panel). For each time point, 12–21 cells were averaged from three independent experiments. FRET E was significantly enhanced at 3 min (ANOVA with Dunnett's post hoc test, **: $0.001 < p < 0.01$). FRET image maps corresponding to the lifetime images above them are shown on the second and third panels. Scalebar: 10 μm. [Colour figure can be viewed at wileyonlinelibrary.com]

fit to a model function incorporating three diffusing components and a triplet transition. The time derivative of the autocorrelation function (Figure 4B inset) helps identify the diffusing components, which in our case were the following: There was a very fast, 3D diffusion component that was attributed to free fluorescent Fab fragments that dissociate from the target HER2 during the measurement. The τ_1 diffusion correlation time of this component was corroborated in experiments with the labeling antibody solution (Figure 4B, dashed trace). In labeled cells, there were at least two 2-dimensional membrane components, of which the faster was attributed to monomers or smaller oligomers, while the slower one was attributed to larger oligomers. This fraction could be occasionally split into a faster and a slower sub-fraction, as demonstrated in the inset, but these were not incorporated into the model to avoid overfitting, and a single τ_3 diffusion correlation time and Φ_3 diffusing fraction were determined for each fitted curve.

The time dependence of the τ_3 diffusion correlation time is plotted in Figure 5A. This diffusion component, characteristic of higher aggregates, increased and then fluctuated considerably in EGF-stimulated cells as compared to mock-stimulated controls (543, 328, 276 and 412 ms vs. 182, 241, 184 and 224 ms at 5, 10, 15 and 20 min post stimulus, respectively). Coherent with the model, the τ_1 and τ_2 diffusion correlation times describing the free label and the smallest diffusing HER2 unit did not change; only their relative fractions varied as a function of cell state.

Based on these data, we assumed a continuous redistribution of membrane-HER2, which was enhanced and shifted toward oligomerization/aggregation by EGF. This assumption was further supported by data pooled from the first 5, the first 25, and beyond 25 min post-stimulus time intervals indicated as B/1, B/2, and B/3 and plotted in the corresponding panels of

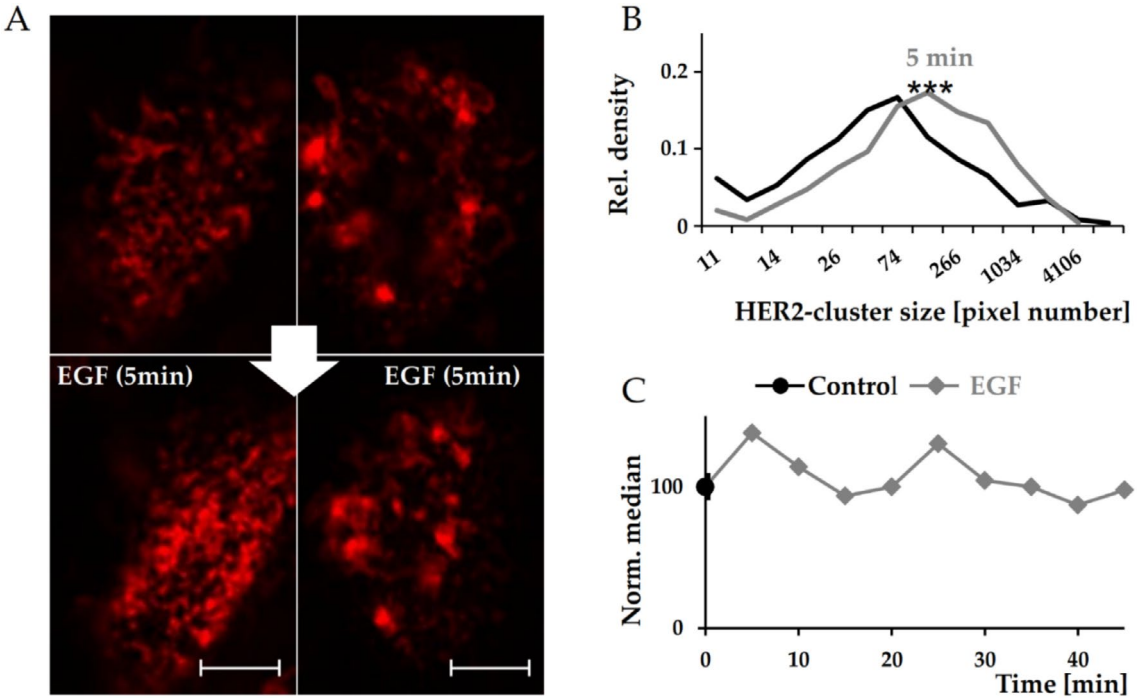

FIGURE 2 | Large scale aggregation dynamics of transactivated HER2. Airyscan superresolution images were acquired from the top membrane slice of cells and processed to determine the cluster size distribution of HER2 molecules labeled with Cy3 conjugated 76.5 Fab. (A) Two pairs of representative images, before and 5 min after adding EGF. Scalebar: 20 μm. (B) Pixel-size distributions of HER2 containing clusters before (black line) and 5 min after EGF stimulation (gray line). χ^2 test; ***: $p < 0.001$. (C) Medians of cluster sizes of EGF-stimulated cells normalized at each time point to mock stimulated controls. Distributions are pooled from 9 treated and 6 control cells. [Colour figure can be viewed at wileyonlinelibrary.com]

Figure 5 as diffusing fraction Φ versus diffusion correlation time τ. The following correlation times (and relative fractions) were observed. Baseline (black circles recurring in all panels): 2.9 ms (8.6%), 68.6 ms (65%), and 216.2 ms (26.3%). Early EGF response, within 5 min of stimulation (Figure 5B/1): 3.8 ms (13%), 58.6 ms (59.8%), and 579 ms (26.5%). Here, the most relevant change is the significant lengthening of the diffusion time of slow HER2 clusters indicating rapid aggregation in the membrane. This aggregation is strongly supported by the increase of the median brightness of diffusing units from 3 to 6 and the shifting of the photon counting histogram to the right (Figure 5C). Long-term initial EGF response within 25 min of stimulation (Figure 5B/2) yielded 1.6 ms (12%), 61 ms (69%), and 390 ms (19%). Here, the fraction of basic HER2 diffusion units (monomers/dimers) increases compared to the initial 5 min, while the fraction of higher aggregates decreases, which can be explained by EGF-induced internalization followed by recycling of HER2 basic diffusion units. The internalization of the larger aggregates also reduces their average diffusion time, but this is still elongated compared to baseline. From 25 min post-EGF stimulation and beyond, the correlation times and the corresponding diffusing fractions reach a new equilibrium similar to that of the unstimulated condition (Figure 5B/3): 1.8 ms (22%), 62 ms (32%), and 227 ms (46%). The increased fraction of shed labels (22%) is explained by the longer time spent under observation, while the increased fraction of larger HER2 aggregates is probably present at the cost of the decreased fraction of basic diffusing HER2 units, and more time would be needed to reach baseline again.

3.5 | Fluorescence Cross-Correlation Spectroscopy (FCCS) Reveals Enhanced Stable Co-Diffusion of HER2 in EGF-Stimulated Cells

The relative fractions, diffusion properties, and stability of co-diffusing di- and oligomers were monitored by dual-color fluorescence cross-correlation spectroscopy (FCCS). For this purpose, membrane-localized HER2 was mixed with a mixture of AF488 or AF647 conjugated Fab 76.5 so that each HER2 molecule was either labeled with AF488 or AF647. This allowed the detection of correlated fluctuations in the two spectral channels for cases when two distinctly labeled species entered and exited the confocal volume together (Figure 6A). Such correlation was readily detected after the addition of EGF when plotting the count rate of the AF647 channel against that of the AF488 channel for each time point along the fluctuation curve (Figure 6B). For control, the number of stably co-diffusing species in the observation volume was calculated in two ways, relating both 488 nm-excited emission to 633 nm-excited emission at various τ intervals (488 vs. 633) and vice versa (633 vs. 488, see at Equation 12). These numbers were then normalized to the number of diffusing species excited at 488 nm, and, for control, also to the number of those excited at 633 nm. For all four of the obtained values, one expects similar results, which are slightly influenced by the diverse quantum efficiencies and detection efficacies and could be biased by the non-perfect overlap of 488 nm- and 633 nm-excited confocal volumes. Figure 6C shows these values as mean ± SEM for the mock-stimulated and the EGF-stimulated cells inside the

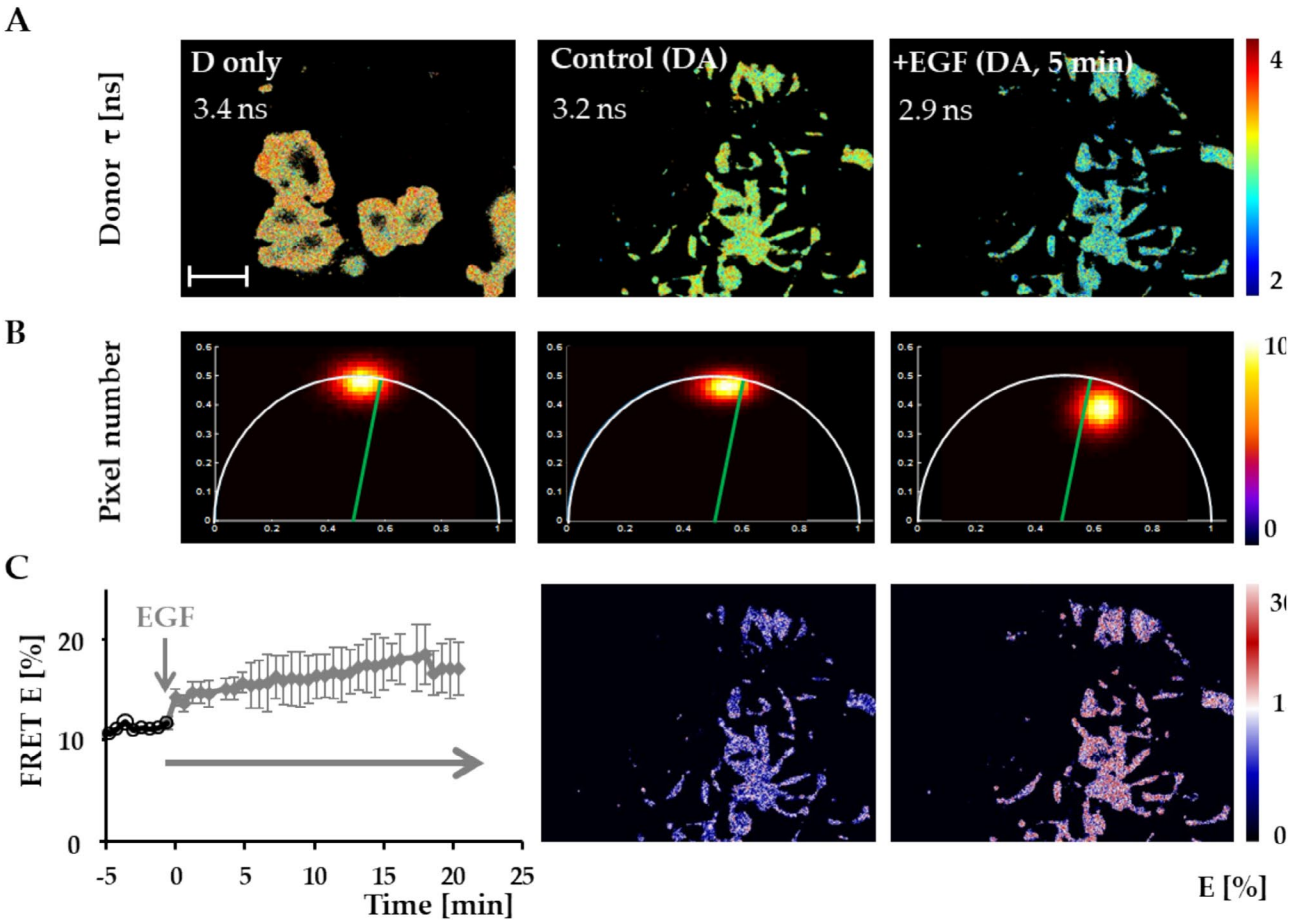

FIGURE 3 | HER2-HER2 molecular interaction monitored by fd-FLIM-FRET. HER2-HER2 molecular proximity and EGF-induced increase in homoassociation were investigated by monitoring FRET efficiency calculated from the shortening of donor lifetime (τ) in the presence of acceptor. Images were taken in a widefield frequency-domain fluorescence lifetime imaging microscope (fd-FLIM FRET). HER2 was labeled with a mixture of Fab antibody fragments targeted to the same epitope and conjugated with either AF488 (serving as donor) or Cy3 (serving as acceptor). (A) Panels show representative images of the observed donor lifetime based on the phase shift of emission: Donor only, donor + acceptor control, donor + acceptor sample 5 min after EGF treatment. The color-coded bars on the left side of the panels indicate pixelwise donor lifetime values. Scalebar: 20 μm. (B) Phasor plot representations of donor lifetime calculated from phase-shift/modulation-depth changes showing significantly increased interaction between HER2 molecules upon EGF binding. The color code represents pixel numbers at each coordinate of the plot. (C) The time dependence of average cellular FRET efficiency values is plotted in the first panel as mean ± SD for 9 cells (1–3 cells measured in each of four independent experiments). The last two panels show the FRET E distribution maps calculated from the respective donor lifetime images shown above them in (A). The color-coded bar on the right represents FRET efficiency scale. [Colour figure can be viewed at wileyonlinelibrary.com]

5 min interval after the stimulus. The addition of EGF causes a significant increase in the relative fractions of co-diffusing species, supporting the previous notion that transactivation enhances HER2 homo-aggregation and establishing that this interaction is stable for at least the time span of the diffusion correlation time.

3.6 | EGF Stimulus Evokes Phosphorylation of EGFR and HER2

As a functional correlate of EGF-evoked transactivation, receptor phosphorylation was monitored by Western blotting. For reference, both total and phospho-receptors were analyzed, and relative phosphorylation was also calculated from the ECL images. Both the native images and their quantitative analysis corroborate EGF-induced EGFR (Figure 7A) and HER2 (Figure 7B) phosphorylation without major changes in total receptor numbers on the 10-min timescale, which verifies transactivation and the functional connection between EGFR and HER2 in SK-BR-3 cells.

4 | Discussion

In early studies, spontaneous dimerization of HER2 was assumed in receptor-overexpressing cells [66, 67]. In transfected cells, homo- and heteroassociation of membrane-HER2 may exist ligand-independently [68]. Also, with recent modern techniques, data of assumed spontaneous HER2 homodimers have been continuously gathered on fixed cells [69–71]. According to literature data, dynamic equilibria may exist among monomer, dimer, and oligomer states of EGFR [8]. Several previous studies [72] proved that EGFR is partly in dimeric/oligomeric states even without stimulus [73–77]. Induced dimer-tetramer state transition has also been proposed [78].

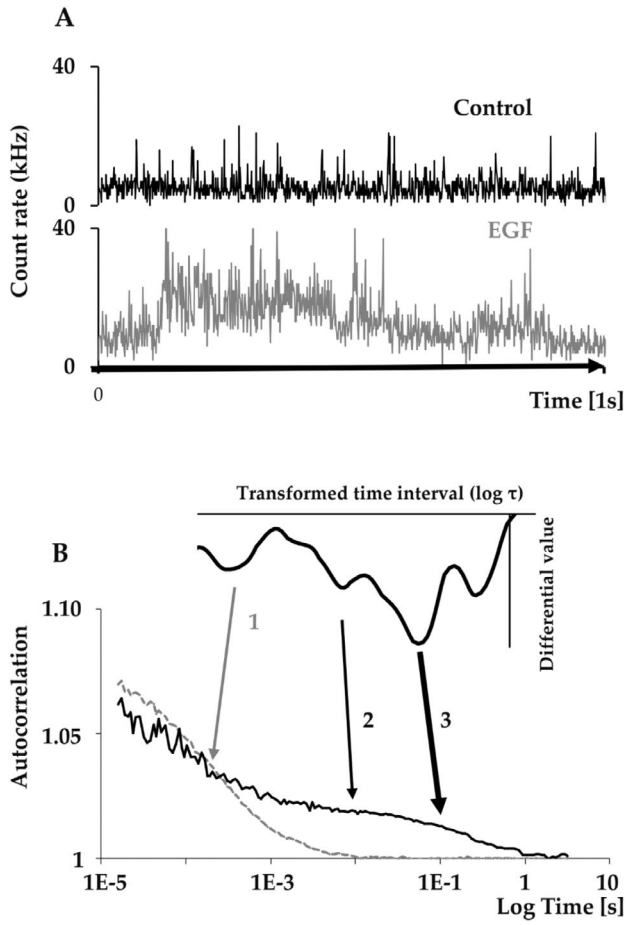

FIGURE 4 | Co-existing membrane HER2-subpopulations with different diffusion characteristics revealed by FCS. (A) Fluorescence species of labeled HER2 enter into and exit from the subfemtoliter excitation/detection volume positioned in the upper cell membrane (solid black line). EGF causes formation of HER2 oligomers and higher-order aggregates increasing the amplitude and altering the pattern of fluorescence fluctuation (gray line). (B) The autocorrelation function of the free, fluorescently conjugated Fabs is represented by the dashed line. On autocorrelation curves from labeled cell membranes, in addition to the free Fabs, the membrane localized HER2 appears in the right-shifted part of the curve (solid black line). The inflection points of this curve indicate the various characteristic diffusion times of the various labeled molecular species. The insert shows a Savietzky-Golay filtered time-derivative of the black autocorrelation curve, where the local minima correspond to the inflection points and help visually identify the potential characteristic diffusion times of various components. Applying this approach, the distinguishable co-existing fractions were the following: (1) a quick, 3D diffusion, attributed to free fluorescently conjugated Fab antibody fragments in the solution (dashed line), and corresponding to the dissociated labels in cellular samples (solid black line, arrow 1, τ_1). (2) A fast-membrane fraction diffusing in 2D, corresponding to labeled monomers/smaller oligomers (arrow 2, τ_2) and (3) a slow-membrane fraction diffusing in 2D corresponding to larger oligomers/mobile aggregates (arrow 3, τ_3).

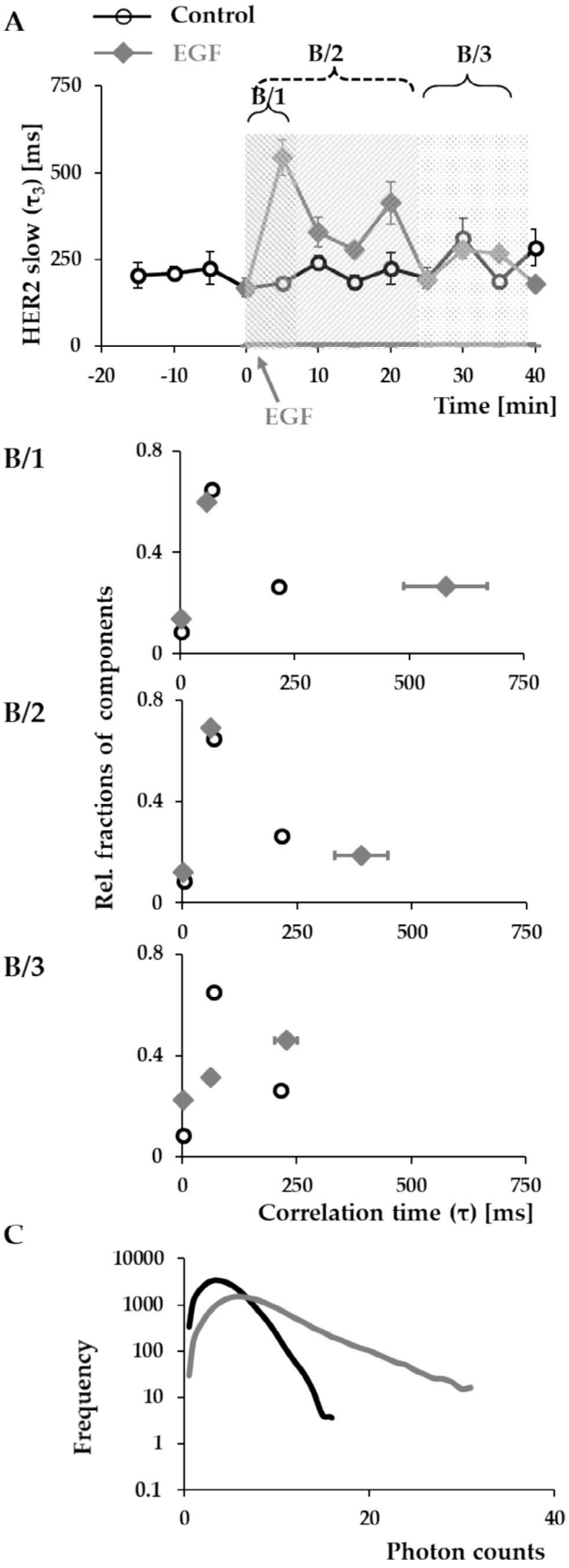

FIGURE 5 | Legend on next page.

It is believed that oligomerization promotes EGFR kinase activation and trans-phosphorylation [68, 77–80]. Ligand-dependent and independent aggregation may ensue owing to different portions of the extracellular, transmembrane, and kinase domains and may yield different types and degrees of kinase activity of EGFR [81]. Localization of consequential signaling platforms may also have a significant effect on receptor sequestration, recycling, degradation, and the binding of effectors and adapters

FIGURE 5 | Redistribution of co-existing membrane fractions of HER2 after EGF stimulation. (A) Diffusion correlation times of the slow HER2 component (τ_3) as a function of time upon EGF stimulation. Fitted data were pooled into 5 min intervals, $t = 0$ marking the time of stimulation. Maximum increase at 5 min after stimulus is 543 ± 81 ms. (B) Distribution of diffusion correlation times and their relative frations in control (black circles, $n > 11$ per time point) and stimulated (gray diamonds, $n > 8$ per time point) as mean ± SEM. (B/1) The first 5 min interval is pooled after EGF treatment. (B/2) Data pooled during the first 25 min of EGF-response. (B/3) Data from 25 min post-EGF and beyond. (C) Representative photon count histograms from mock stimulated (black line) and EGF stimulated cells at the 5 min time point.

[2, 9]. Importantly, similar mechanisms regulate not only all HER homodimers but also their heterodimers [75].

HER2 is a preferred heterodimerization partner of all HER family members, including EGFR [2]. Their interaction is crucial in cancer development. While HER2 overexpression alone may not lead to hyper-autophosphorylation, the presence of other HERs can alter signaling patterns. Particularly, the EGFR-HER2 interaction could lead to sustained HER signaling [10].

However, the details of EGFR-HER2 interaction, primarily the dynamics and stoichiometry of ligand-driven aggregation and signaling in situ in living cells, are still not fully understood. Here, we performed a systematic investigation with various fluorescence-based techniques in order to reveal the interrelated time courses of hetero- and homoassociations, oligomerization, and cluster formation of HER2 on SK-BR-3, a clinically highly relevant breast cancer cell line that expresses not only HER2 at high levels but also EGFR at moderate levels [58, 59].

To decipher the spatiotemporal relationships of EGFR-HER2 interactions, first we investigated the basal and EGF-induced heteroassociations between EGFR and HER2 molecules using time-domain fluorescence lifetime imaging microscopy (td-FLIM) and determined the FRET efficiency between the donor and acceptor labeled monoclonal antibodies tagging the membrane-embedded receptors. The measured FRET efficiency between EGFR and HER2 revealed a basal level of communication between them, which was further increased by EGF stimulation within 2 and 3 min. Later, the EGF-induced transiently enhanced interaction of EGFR and HER2 was gradually decreased to baseline by 10 min (Figures 1C and 8). The functional outcomes of EGF-induced transactivation included the phosphorylation of both receptors (Figures 7 and 8). Interestingly, the phosphorylation event seems to have a faster kinetics than the increase in FRET efficiency, suggesting that the "ignition" of enhanced phosphorylation can be achieved by a smaller number of heteroassociations between EGFR and HER2. Western Blot analysis also revealed that significant HER2 autophosphorylation was also present on SK-BR-3 without EGF. This observation suggests that overexpressed HER2 does in fact induce basal signaling without transactivation in cancers. This renders the use of HER2 kinase inhibitors such as tucatinib, neratinib, and lapatinib [82] relevant as an adjuvant, even for cases where by targeting HER2 with antibodies such as trastuzumab or pertuzumab,

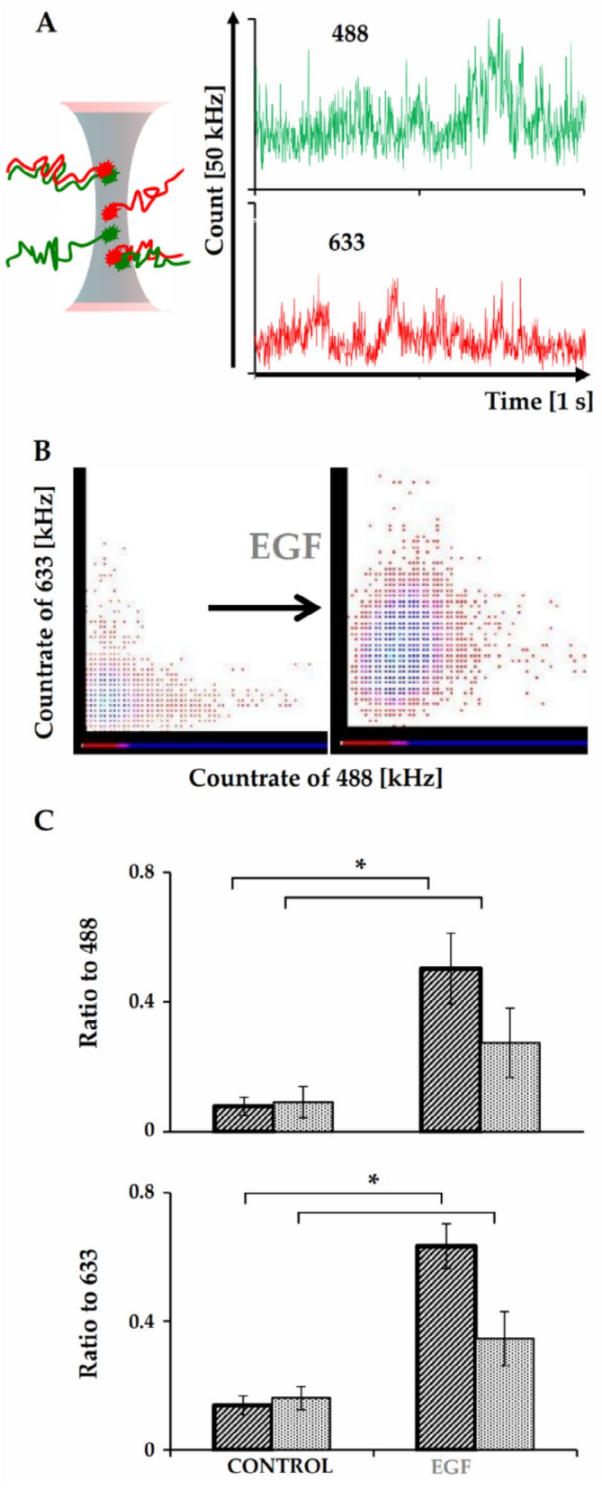

FIGURE 6 | Legend on next page.

the major effect is expected through ADCC [83, 84], or when using antibody-drug conjugates such as T-DM1 or trastuzumab deruxtecan, through tumor-selective cytotoxicity [82].

EGF induced EGFR-HER2 interaction was almost concomitantly followed by enhanced interaction of HER2 molecules with each other. This was manifested on multiple scales. At the level of individual receptors, their increased homoassociation was

FIGURE 6 | Stable co-diffusion of HER2 molecules is enhanced upon EGF stimulation. Fluctuation of fluorescence signals from membrane HER2 labeled with a mixture AF488 and AF647 conjugated 76.5 monoclonal Fab was analyzed for crosscorrelation. (A) Diffusion of distinctly labeled fluorescent species across the confocal volume can give rise to both correlated and uncorrelated emission depending on the stability of interaction between the diffusing molecules. (B) Plotting the count rate of the two distinct fluorescent signals for each time point on a color dot-plot reveals enhanced correlation between them after EGF stimulation, a result of stabilized interaction between the labeled species. (C) The number of slowly co-diffusing species was calculated both from using channel 1 (488 nm excitation, dark gray columns) and channel 2 (633 nm excitation, light gray columns) as reference (see Equation 12). These were normalized to the number of diffusing AF488 labeled species (top graph) or to the AF637 labeled species (bottom graph). Data from control ($n = 18$) and stimulated ($n = 8$) cells acquired within 5 min of EGF stimulation are plotted as mean ± SEM. *: $p < 0.05$. [Colour figure can be viewed at wileyonlinelibrary.com]

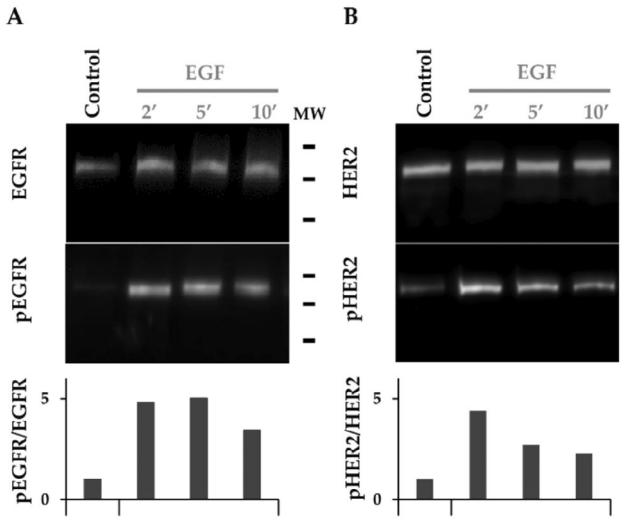

FIGURE 7 | Functional consequences of EGF-induced transactivation as revealed by Western blotting. Total and phosphorylated EGFR (panel A) and HER2 (panel B) were detected by ECL after Western blotting of cell lysates prepared at the indicated 2, 5, and 10 min after adding EGF and compared to unstimulated control. Signal from each luminescent spot was measured and integrated in ImageJ/FIJI, and the ratio of phosphorylated to total receptor signal was plotted for each time point of both pairs of the blot images.

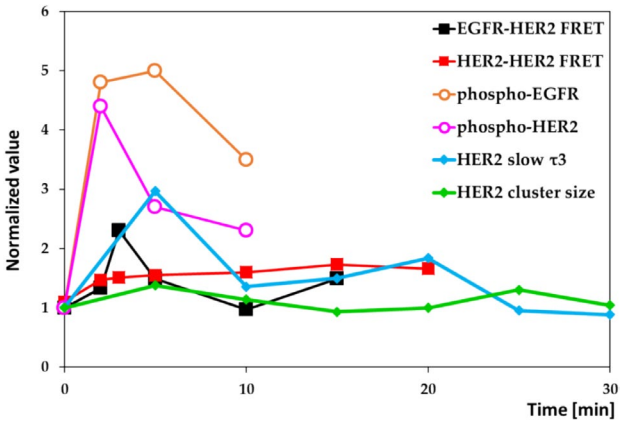

FIGURE 8 | Temporal pattern of EGF-induced HER protein hetero- and homoassociations, phosphorylation, and oligomer formation. The most prominent time-wise changes presented in figures the results EGFR-HER2 FRET were measured with time-domain FLIM in confocal membrane slices of cells fixed at different time points after stimulus. HER2-HER2 FRET was assessed in live cells using widefield frequency-domain FLIM encompassing the whole cell. EGFR and HER2 phosphorylation were measured in Western blot images. The diffusion correlation time of HER2 aggregates in the membrane (slow τ_3) was quantified in 5-min time windows after stimulus with fluorescence correlation spectroscopy. Stationary and extremely slow-moving large HER2 membrane clusters were measured by Airyscan superresolution microscopy. Phosphorylated receptor levels were normalized to total receptor levels; all other parameters were normalized to the corresponding untreated control at the same time point. [Colour figure can be viewed at wileyonlinelibrary.com]

revealed by frequency domain FLIM measurements (Figures 3C and 8A). Since SK-BR-3 cells express about 800,000 HER2 on the cell surface, frequency domain FLIM FRET could be used to monitor the time course of HER2 homoassociation in live cells for up to 25 min. While heteroassociation between EGFR and HER2 returned to the basal level within 10 min, the increased HER2 homoassociation was steady for at least 20 min. This apparently different dynamics for HER2-HER2 interaction is explained by the fact that the fd-FLIM measurements were done in widefield mode, encompassing not only the cell membrane but also the intracellular space, and thus reporting about interactions also in internalized membrane vesicles. In fact, using Airyscan superresolution microscopy, which was restricted to a thin slice of the cell membrane, revealed that submicron scale aggregation of membrane-localized HER2 first increases, just as FRET efficiency between HER2 molecules (Figures 2C vs. 3C, and 8), but then fluctuates to decrease and increase again, similarly to EGFR-HER2 FRET measured exclusively in the cell membrane with confocal td-FLIM (Figures 1C and 8). It should be noted that this measurement only assesses correctly the clusters that have sizes over the resolution limit and thus overestimates the average cluster size. However, it is still useful for revealing changes in higher order meso-scale receptor aggregation which is not accessible by dynamic methods such as correlation spectroscopy. While this latter approach is insensitive to stationary or slowly moving clusters, it excels in characterizing diffusible entities and their mobile aggregates.

Thus, to gain coherent information on both the molecular level associations and the higher level aggregation of HER2 in the cell membrane, we have also applied fluorescence correlation and cross-correlation spectroscopy (FCS/FCCS). FCS and FCCS are a sensitive tools for monitoring altered diffusion properties of fluorescently labeled molecules entering and exiting a confocal volume. This volume can be positioned so that its intersection with the cell membrane selects a defined area for quantifying mobility, aggregation, and absolute concentration of membrane proteins in a single measurement [47]. In our cellular model, the time-derivative of the autocorrelation function hinted at a the presence of a basic diffusion unit of HER2 and at least one aggregated component even in unstimulated cells, in addition to the detached Fab labels and the unavoidable triplet transition of the dyes (Figure 4). The slow diffusion correlation time

characterizing the aggregated mobile clusters of HER2 has exhibited an EGF-induced lengthening reaching its first peak at 5 min, then showing cyclic increases and decreases reaching a new equilibrium over some 40 min (Figures 5 and 8). These cyclic changes, paralleled by similar ones in the size of stationary large clusters (Figures 2 and 8) could be attributed to internalization and partial recycling of HER2, as hinted by the long-term reduction of the fraction of basic HER2 diffusion units (Figure 5B/3).

Importantly, the highest level of HER2 aggregation at 5 min after EGF stimulus, in addition to the drastic dwindling of diffusion speed, has been corroborated by two other techniques. First, photon count histograms constructed from fluctuation signals revealed that both the mode and the maximum of the size distribution of diffusing units doubled upon stimulus (Figure 5C). Second, fluorescence cross-correlation spectroscopy (FCCS) has demonstrated that the fraction of HER2 molecules that stably interact and co-diffuse for at least the duration of time spent in the confocal observation volume significantly increased (Figure 6). The FCCS approach was particularly valuable here as, in contrast to FRET measurements that serve a snapshot of interacting molecules without evaluating time-wise stability, it supplied evidence of the longer-term binding between HER2 molecules during the phase of most extensive aggregation. This implies a prolonged inaccessibility to the therapeutic pertuzumab (Perjeta), designed to inhibit HER2 dimerization and activation by binding to the receptor's dimerization arm [85].

Overall, the complementary array of state-of-the-art imaging cytometry approaches thus demonstrates a spatiotemporal pattern of spontaneous and induced aggregation states of HER2 modulated by the presence of ligand-bound EGFR, which could provide mechanistic insights into the potential success of targeted therapies directed to the HER family of receptor tyrosine kinases. Of particular significance, the time course of both EGFR-HER2 heteroassociation and the degree of HER2 homoclustering suggests that in the case of EGFR-triggered HER2 transactivation there may be time-windows when the therapeutic antibody pertuzumab can more efficiently bind to its target and exert its effect. This may be highly relevant to the clinic as until now it has not been investigated how the expression of EGFR influences the therapeutic outcome in HER2-positive tumors. However, when translating these results to preclinical models, the complexity of the in vivo tumor microenvironment would also need to be taken into account. The time-dependent changes of the local concentration of EGFR ligands, including variations of intrans presented juxtacrine stimuli [86], the effect of membrane cholesterol content on the rate of EGFR internalization [87], the density of membrane-anchored sialomucins modulating HER2 activation [88] and the presence of other members of the HER family and their specific ligands [1, 2] may all modulate the dynamics of EGFR and HER2 homo- and heteroassociations.

Author Contributions

László Ujlaky-Nagy: conceptualization, investigation, writing – original draft, methodology, visualization, formal analysis, data curation. **János Szöllősi:** conceptualization, writing – review and editing, writing – original draft, supervision, resources, funding acquisition. **György Vereb:** conceptualization, funding acquisition, writing – original draft, methodology, visualization, writing – review and editing, project administration, supervision, resources.

Acknowledgments

We acknowledge the financial support from GINOP-2.3.3-15-2016-00003 (co-financed by the European Union and the European Regional Development Fund), NKFIH OTKA K143771 (the National Research, Development, and Innovation Office, Hungary), the HUN-REN Hungarian Research Network, and the University of Debrecen Program for Scientific Publication.

Conflicts of Interest

The authors declare no conflicts of interest.

Data Availability Statement

Data pertinent to the research are included in the article. The raw data that support the findings of this study are available from the corresponding author upon reasonable request.

References

1. Y. Yarden and G. Pines, "The ERBB Network: At Last, Cancer Therapy Meets Systems Biology," *Nature Reviews. Cancer* 12 (2012): 553–563.

2. Y. Yarden and M. X. Sliwkowski, "Untangling the ErbB Signalling Network," *Nature Reviews. Molecular Cell Biology* 2 (2001): 127–137.

3. J. Han, Y. Zhang, J. Xu, et al., "Her4 Promotes Cancer Metabolic Reprogramming via the c-Myc-Dependent Signaling Axis," *Cancer Letters* 496 (2021): 57–71.

4. M. I. El-Gamal, N. H. Mewafi, N. E. Abdelmotteleb, et al., "A Review of HER4 (ErbB4) Kinase, Its Impact on Cancer, and Its Inhibitors," *Molecules* 26, no. 23 (2021): 7376, https://doi.org/10.3390/molecules26237376.

5. G. Brockhoff, "Shedding Light on HER4 Signaling in Normal and Malignant Breast Tissues," *Cellular Signalling* 97 (2022): 110401.

6. S. R. Needham, S. K. Roberts, A. Arkhipov, et al., "EGFR Oligomerization Organizes Kinase-Active Dimers Into Competent Signalling Platforms," *Nature Communications* 7 (2016): 13307.

7. H. Yamashita, Y. Yano, K. Kawano, and K. Matsuzaki, "Oligomerization-Function Relationship of EGFR on Living Cells Detected by the Coiled-Coil Labeling and FRET Microscopy," *Biochimica et Biophysica Acta* 1848 (2015): 1359–1366.

8. I. Chung, R. Akita, R. Vandlen, D. Toomre, J. Schlessinger, and I. Mellman, "Spatial Control of EGF Receptor Activation by Reversible Dimerization on Living Cells," *Nature* 464 (2010): 783–787.

9. A. Sorkin and M. Von Zastrow, "Signal Transduction and Endocytosis: Close Encounters of Many Kinds," *Nature Reviews. Molecular Cell Biology* 3 (2002): 600–614.

10. N. E. Hynes and G. MacDonald, "ErbB Receptors and Signaling Pathways in Cancer," *Current Opinion in Cell Biology* 21 (2009): 177–184.

11. S. Y. Lee, M. J. Kim, G. Jin, et al., "Somatic Mutations in Epidermal Growth Factor Receptor Signaling Pathway Genes in Non-Small Cell Lung Cancers," *Journal of Thoracic Oncology* 5 (2010): 1734–1740.

12. H. Shigematsu and A. F. Gazdar, "Somatic Mutations of Epidermal Growth Factor Receptor Signaling Pathway in Lung Cancers," *International Journal of Cancer* 118 (2006): 257–262.

13. N. E. Hynes and T. Schlange, "Targeting ADAMS and ERBBs in Lung Cancer," *Cancer Cell* 10 (2006): 7–11.

14. S. V. Sharma and J. Settleman, "ErbBs in Lung Cancer," *Experimental Cell Research* 315 (2009): 557–571.

15. T. P. Garrett, N. M. McKern, M. Lou, et al., "The Crystal Structure of a Truncated ErbB2 Ectodomain Reveals an Active Conformation, Poised to Interact With Other ErbB Receptors," *Molecular Cell* 11 (2003): 495–505.

16. K. M. Ferguson, M. B. Berger, J. M. Mendrola, H. S. Cho, D. J. Leahy, and M. A. Lemmon, "EGF Activates Its Receptor by Removing Interactions That Autoinhibit Ectodomain Dimerization," *Molecular Cell* 11 (2003): 507–517.

17. A. W. Burgess, H. S. Cho, C. Eigenbrot, et al., "An Open-And-Shut Case? Recent Insights Into the Activation of EGF/ErbB Receptors," *Molecular Cell* 12 (2003): 541–552.

18. T. P. Garrett, N. M. McKern, M. Lou, et al., "Crystal Structure of a Truncated Epidermal Growth Factor Receptor Extracellular Domain Bound to Transforming Growth Factor Alpha," *Cell* 110 (2002): 763–773.

19. H. Ogiso, R. Ishitani, O. Nureki, et al., "Crystal Structure of the Complex of Human Epidermal Growth Factor and Receptor Extracellular Domains," *Cell* 110 (2002): 775–787.

20. D. J. Slamon, G. M. Clark, S. G. Wong, W. J. Levin, A. Ullrich, and W. L. McGuire, "Human Breast Cancer: Correlation of Relapse and Survival With Amplification of the HER-2/Neu Oncogene," *Science* 235 (1987): 177–182.

21. I. Marrocco and Y. Yarden, "Resistance of Lung Cancer to EGFR-Specific Kinase Inhibitors: Activation of Bypass Pathways and Endogenous Mutators," *Cancers (Basel)* 15, no. 20 (2023): 5009.

22. H. Zhang, B. S. Finkelman, M. G. Ettel, M. J. Velez, B. M. Turner, and D. G. Hicks, "HER2 Evaluation for Clinical Decision Making in Human Solid Tumours: Pearls and Pitfalls," *Histopathology* 85 (2024): 3–19.

23. J. Carlsson, K. Wester, M. De La Torre, P. U. Malmstrom, and T. Gardmark, "EGFR-Expression in Primary Urinary Bladder Cancer and Corresponding Metastases and the Relation to HER2-Expression. On the Possibility to Target These Receptors With Radionuclides," *Radiology and Oncology* 49 (2015): 50–58.

24. R. Horii, H. Nitta, M. Nojima, et al., "Predictive Significance of HER2 Intratumoral Heterogeneity, Determined by Simultaneous Gene and Protein Analysis, for Resistance to Trastuzumab-Based Treatments for HER2-Positive Breast Cancer," *Virchows Archiv* 479 (2021): 13–21.

25. O. M. Filho, G. Viale, S. Stein, et al., "Impact of HER2 Heterogeneity on Treatment Response of Early-Stage HER2-Positive Breast Cancer: Phase II Neoadjuvant Clinical Trial of T-DM1 Combined With Pertuzumab," *Cancer Discovery* 11 (2021): 2474–2487.

26. F. Weinberg, D. B. Peckys, and N. de Jonge, "EGFR Expression in HER2-Driven Breast Cancer Cells," *International Journal of Molecular Sciences* 21, no. 23 (2020): 9008, https://doi.org/10.3390/ijms21239008.

27. M. Lim, T. H. Nguyen, C. Niland, et al., "Landscape of Epidermal Growth Factor Receptor Heterodimers in Brain Metastases," *Cancers (Basel)* 14, no. 3 (2022): 533, https://doi.org/10.3390/cancers14030533.

28. M. D. Pegram, A. Lipton, D. F. Hayes, et al., "Phase II Study of Receptor-Enhanced Chemosensitivity Using Recombinant Humanized Anti-p185HER2/Neu Monoclonal Antibody Plus Cisplatin in Patients With HER2/Neu-Overexpressing Metastatic Breast Cancer Refractory to Chemotherapy Treatment," *Journal of Clinical Oncology* 16 (1998): 2659–2671.

29. I. E. Krop, M. Beeram, S. Modi, et al., "Phase I Study of Trastuzumab-DM1, an HER2 Antibody-Drug Conjugate, Given Every 3 Weeks to Patients With HER2-Positive Metastatic Breast Cancer," *Journal of Clinical Oncology* 28 (2010): 2698–2704.

30. D. B. Agus, M. S. Gordon, C. Taylor, et al., "Phase I Clinical Study of Pertuzumab, a Novel HER Dimerization Inhibitor, in Patients With Advanced Cancer," *Journal of Clinical Oncology* 23 (2005): 2534–2543.

31. T. Forster, "Energiewanderung und Fluoreszenz," *Naturwissenschaften* 33 (1946): 166–175.

32. E. A. Jares-Erijman and T. M. Jovin, "FRET Imaging," *Nature Biotechnology* 21 (2003): 1387–1395.

33. G. Vereb, E. Jares-Erijman, P. R. Selvin, and T. M. Jovin, "Temporally and Spectrally Resolved Imaging Microscopy of Lanthanide Chelates," *Biophysical Journal* 74 (1998): 2210–2222.

34. G. Vereb, J. Matko, and J. Szollosi, "Cytometry of Fluorescence Resonance Energy Transfer," *Methods in Cell Biology* 75 (2004): 105–152.

35. J. Roszik, J. Szollosi, and G. Vereb, "AccPbFRET: An ImageJ Plugin for Semi-Automatic, Fully Corrected Analysis of Acceptor Photobleaching FRET Images," *BMC Bioinformatics* 9 (2008): 346.

36. J. Roszik, D. Lisboa, J. Szollosi, and G. Vereb, "Evaluation of Intensity-Based Ratiometric FRET in Image Cytometry–Approaches and a Software Solution," *Cytometry. Part A* 75 (2009): 761–767.

37. P. Bagossi, G. Horvath, G. Vereb, J. Szollosi, and J. Tozser, "Molecular Modeling of Nearly Full-Length ErbB2 Receptor," *Biophysical Journal* 88 (2005): 1354–1363.

38. I. Rebenku, C. B. Lloyd, J. Szollosi, and G. Vereb, "Pixel-By-Pixel Autofluorescence Corrected FRET in Fluorescence Microscopy Improves Accuracy for Samples With Spatially Varied Autofluorescence to Signal Ratio," *Scientific Reports* 13 (2023): 2934.

39. S. Padilla-Parra and M. Tramier, "FRET Microscopy in the Living Cell: Different Approaches, Strengths and Weaknesses," *BioEssays* 34 (2012): 369–376.

40. T. Ungvari, P. Gogolak, M. Bagdany, L. Damjanovich, and L. Bene, "Perrin and Forster Unified: Dual-Laser Triple-Polarization FRET (3polFRET) for Interactions at the Forster-Distance and Beyond," *Biochimica et Biophysica Acta* 1863 (2016): 703–716.

41. D. J. Liput, T. A. Nguyen, S. M. Augustin, J. O. Lee, and S. S. Vogel, "A Guide to Fluorescence Lifetime Microscopy and Forster's Resonance Energy Transfer in Neuroscience," *Current Protocols in Neuroscience* 94 (2020): e108.

42. E. B. van Munster and T. W. Gadella, "Fluorescence Lifetime Imaging Microscopy (FLIM)," *Advances in Biochemical Engineering/Biotechnology* 95 (2005): 143–175.

43. D. M. Grant, J. McGinty, E. J. McGhee, et al., "High Speed Optically Sectioned Fluorescence Lifetime Imaging Permits Study of Live Cell Signaling Events," *Optics Express* 15 (2007): 15656–15673.

44. W. Becker, "Fluorescence Lifetime Imaging–Techniques and Applications," *Journal of Microscopy* 247 (2012): 119–136.

45. E. B. van Munster, J. Goedhart, G. J. Kremers, E. M. Manders, and T. W. Gadella, Jr., "Combination of a Spinning Disc Confocal Unit With Frequency-Domain Fluorescence Lifetime Imaging Microscopy," *Cytometry. Part A* 71 (2007): 207–214.

46. R. Rigler, "Fluorescence Correlations, Single Molecule Detection and Large Number Screening. Applications in Biotechnology," *Journal of Biotechnology* 41 (1995): 177–186.

47. R. Brock, G. Vamosi, G. Vereb, and T. M. Jovin, "Rapid Characterization of Green Fluorescent Protein Fusion Proteins on the Molecular and Cellular Level by Fluorescence Correlation Microscopy," *Proceedings of the National Academy of Sciences of the United States of America* 96 (1999): 10123–10128.

48. P. Schwille, U. Haupts, S. Maiti, and W. W. Webb, "Molecular Dynamics in Living Cells Observed by Fluorescence Correlation Spectroscopy With One- and Two-Photon Excitation," *Biophysical Journal* 77 (1999): 2251–2265.

49. P. Dittrich, F. Malvezzi-Campeggi, M. Jahnz, and P. Schwille, "Accessing Molecular Dynamics in Cells by Fluorescence Correlation Spectroscopy," *Biological Chemistry* 382 (2001): 491–494.

50. S. A. Kim, K. G. Heinze, and P. Schwille, "Fluorescence Correlation Spectroscopy in Living Cells," *Nature Methods* 4 (2007): 963–973.

51. G. Vamosi, E. Friedlander-Brock, S. M. Ibrahim, R. Brock, J. Szollosi, and G. Vereb, "EGF Receptor Stalls Upon Activation as Evidenced by Complementary Fluorescence Correlation Spectroscopy and Fluorescence Recovery After Photobleaching Measurements," *International Journal of Molecular Sciences* 20, no. 13 (2019): 3370.

52. M. Eigen and R. Rigler, "Sorting Single Molecules: Application to Diagnostics and Evolutionary Biotechnology," *Proceedings of the National Academy of Sciences of the United States of America* 91 (1994): 5740–5747.

53. J. D. Muller, Y. Chen, and E. Gratton, "Resolving Heterogeneity on the Single Molecular Level With the Photon-Counting Histogram," *Biophysical Journal* 78 (2000): 474–486.

54. P. Schwille, F. J. Meyer-Almes, and R. Rigler, "Dual-Color Fluorescence Cross-Correlation Spectroscopy for Multicomponent Diffusional Analysis in Solution," *Biophysical Journal* 72 (1997): 1878–1886.

55. K. Bacia, Z. Petrasek, and P. Schwille, "Correcting for Spectral Cross-Talk in Dual-Color Fluorescence Cross-Correlation Spectroscopy," *ChemPhysChem* 13 (2012): 1221–1231.

56. T. Weidemann and P. Schwille, "Dual-Color Fluorescence Cross-Correlation Spectroscopy With Continuous Laser Excitation in a Confocal Setup," *Methods in Enzymology* 518 (2013): 43–70.

57. P. Schwille and K. G. Heinze, "Two-Photon Fluorescence Cross-Correlation Spectroscopy," *ChemPhysChem* 2 (2001): 269–272.

58. M. H. Kraus, N. C. Popescu, S. C. Amsbaugh, and C. R. King, "Overexpression of the EGF Receptor-Related Proto-Oncogene erbB-2 in Human Mammary Tumor Cell Lines by Different Molecular Mechanisms," *EMBO Journal* 6 (1987): 605–610.

59. C. R. King, I. Borrello, F. Bellot, P. Comoglio, and J. Schlessinger, "Egf Binding to Its Receptor Triggers a Rapid Tyrosine Phosphorylation of the erbB-2 Protein in the Mammary Tumor Cell Line SK-BR-3," *EMBO Journal* 7 (1988): 1647–1651.

60. S. Diermeier, G. Horvath, R. Knuechel-Clarke, F. Hofstaedter, J. Szollosi, and G. Brockhoff, "Epidermal Growth Factor Receptor Coexpression Modulates Susceptibility to Herceptin in HER2/Neu Overexpressing Breast Cancer Cells via Specific erbB-Receptor Interaction and Activation," *Experimental Cell Research* 304 (2005): 604–619.

61. S. Ranjit, L. Malacrida, D. M. Jameson, and E. Gratton, "Fit-Free Analysis of Fluorescence Lifetime Imaging Data Using the Phasor Approach," *Nature Protocols* 13 (2018): 1979–2004.

62. R. Datta, T. M. Heaster, J. T. Sharick, A. A. Gillette, and M. C. Skala, "Fluorescence Lifetime Imaging Microscopy: Fundamentals and Advances in Instrumentation, Analysis, and Applications," *Journal of Biomedical Optics* 25 (2020): 1–43.

63. G. Weber, "Resolution of the Fluorescence Lifetimes in a Heterogeneous System by Phase and Modulatlon Measurements," *Journal of Physical Chemistry* 85, no. 8 (1981): 949–953.

64. E. Gratton, D. M. Jameson, and R. D. Hall, "Multifrequency Phase and Modulation Fluorometry," *Annual Review of Biophysics and Bioengineering* 13 (1984): 105–124.

65. Z. Petrasek, J. Ries, and P. Schwille, "Scanning FCS for the Characterization of Protein Dynamics in Live Cells," *Methods in Enzymology* 472 (2010): 317–343.

66. R. M. Hudziak, J. Schlessinger, and A. Ullrich, "Increased Expression of the Putative Growth Factor Receptor p185HER2 Causes Transformation and Tumorigenesis of NIH 3T3 Cells," *Proceedings of the National Academy of Sciences of the United States of America* 84 (1987): 7159–7163.

67. P. P. Di Fiore, J. H. Pierce, M. H. Kraus, O. Segatto, C. R. King, and S. A. Aaronson, "erbB-2 Is a Potent Oncogene When Overexpressed in NIH/3T3 Cells," *Science* 237 (1987): 178–182.

68. P. O. Byrne, K. Hristova, and D. J. Leahy, "EGFR Forms Ligand-Independent Oligomers That Are Distinct From the Active State," *Journal of Biological Chemistry* 295 (2020): 13353–13362.

69. I. N. Dahmke, P. Trampert, F. Weinberg, Z. Mostajeran, F. Lautenschlager, and N. de Jonge, "Correlative Fluorescence- and Electron Microscopy of Whole Breast Cancer Cells Reveals Different Distribution of ErbB2 Dependent on Underlying Actin," *Frontiers in Cell and Development Biology* 8 (2020): 521.

70. D. B. Peckys and N. de Jonge, "Studying the Stoichiometry of Epidermal Growth Factor Receptor in Intact Cells Using Correlative Microscopy," *Journal of Visualized Experiments* 11, no. 103 (2015): 53186.

71. D. B. Peckys, D. Gaa, and N. de Jonge, "Quantification of EGFR-HER2 Heterodimers in HER2-Overexpressing Breast Cancer Cells Using Liquid-Phase Electron Microscopy," *Cells* 10, no. 11 (2021): 3244, https://doi.org/10.3390/cells10113244.

72. A. J. M. Wollman, C. Fournier, I. Llorente-Garcia, et al., "Critical Roles for EGFR and EGFR-HER2 Clusters in EGF Binding of SW620 Human Carcinoma Cells," *Journal of the Royal Society Interface* 19 (2022): 20220088.

73. J. Ichinose, M. Murata, T. Yanagida, and Y. Sako, "EGF Signalling Amplification Induced by Dynamic Clustering of EGFR," *Biochemical and Biophysical Research Communications* 324 (2004): 1143–1149.

74. A. H. Clayton, M. L. Tavarnesi, and T. G. Johns, "Unligated Epidermal Growth Factor Receptor Forms Higher Order Oligomers Within Microclusters on A431 Cells That Are Sensitive to Tyrosine Kinase Inhibitor Binding," *Biochemistry* 46 (2007): 4589–4597.

75. R. H. Tao and I. N. Maruyama, "All EGF(ErbB) Receptors Have Preformed Homo- and Heterodimeric Structures in Living Cells," *Journal of Cell Science* 121 (2008): 3207–3217.

76. P. Nagy, J. Claus, T. M. Jovin, and D. J. Arndt-Jovin, "Distribution of Resting and Ligand-Bound ErbB1 and ErbB2 Receptor Tyrosine Kinases in Living Cells Using Number and Brightness Analysis," *Proceedings of the National Academy of Sciences of the United States of America* 107 (2010): 16524–16529.

77. N. Kozer, D. Barua, S. Orchard, et al., "Exploring Higher-Order EGFR Oligomerisation and Phosphorylation–A Combined Experimental and Theoretical Approach," *Molecular BioSystems* 9 (2013): 1849–1863.

78. A. H. Clayton, F. Walker, S. G. Orchard, et al., "Ligand-Induced Dimer-Tetramer Transition During the Activation of the Cell Surface Epidermal Growth Factor Receptor-A Multidimensional Microscopy Analysis," *Journal of Biological Chemistry* 280 (2005): 30392–30399.

79. Y. Yarden and J. Schlessinger, "Self-Phosphorylation of Epidermal Growth Factor Receptor: Evidence for a Model of Intermolecular Allosteric Activation," *Biochemistry* 26 (1987): 1434–1442.

80. Y. Yarden and J. Schlessinger, "Epidermal Growth Factor Induces Rapid, Reversible Aggregation of the Purified Epidermal Growth Factor Receptor," *Biochemistry* 26 (1987): 1443–1451.

81. Y. Huang, S. Bharill, D. Karandur, et al., "Molecular Basis for Multimerization in the Activation of the Epidermal Growth Factor Receptor," *eLife* 5 (2016): e14107.

82. A. G. Waks, O. Martinez-Saez, P. Tarantino, et al., "Dual HER2 Inhibition: Mechanisms of Synergy, Patient Selection, and Resistance," *Nature Reviews. Clinical Oncology* 21 (2024): 818–832.

83. G. Toth, A. Szoor, L. Simon, Y. Yarden, J. Szollosi, and G. Vereb, "The Combination of Trastuzumab and Pertuzumab Administered at Approved Doses May Delay Development of Trastuzumab Resistance by Additively Enhancing Antibody-Dependent Cell-Mediated Cytotoxicity," *MAbs* 8 (2016): 1361–1370.

84. M. Barok, J. Isola, Z. Palyi-Krekk, et al., "Trastuzumab Causes Antibody-Dependent Cellular Cytotoxicity-Mediated Growth Inhibition of Submacroscopic JIMT-1 Breast Cancer Xenografts Despite

Intrinsic Drug Resistance," *Molecular Cancer Therapeutics* 6 (2007): 2065–2072.

85. M. C. Franklin, K. D. Carey, F. F. Vajdos, D. J. Leahy, A. M. de Vos, and M. X. Sliwkowski, "Insights Into ErbB Signaling From the Structure of the ErbB2-Pertuzumab Complex," *Cancer Cell* 5 (2004): 317–328.

86. J. Dong, L. K. Opresko, W. Chrisler, et al., "The Membrane-Anchoring Domain of Epidermal Growth Factor Receptor Ligands Dictates Their Ability to Operate in Juxtacrine Mode," *Molecular Biology of the Cell* 16 (2005): 2984–2998.

87. N. Bag, S. Huang, and T. Wohland, "Plasma Membrane Organization of Epidermal Growth Factor Receptor in Resting and Ligand-Bound States," *Biophysical Journal* 109 (2015): 1925–1936.

88. M. Liberelle, N. Jonckheere, P. Melnyk, I. Van Seuningen, and N. Lebegue, "EGF-Containing Membrane-Bound Mucins: A Hidden ErbB2 Targeting Pathway?," *Journal of Medicinal Chemistry* 63 (2020): 5074–5088.